Monthly Notices
of the
ROYAL ASTRONOMICAL SOCIETY

Mon. Not. R. Astron. Soc. **402,** 1161–1170 (2010) doi:10.1111/j.1365-2966.2009.15944.x

Polarized QPOs from the *INTEGRAL* polar IGRJ14536-5522 (=Swift J1453.4-5524)

Stephen B. Potter,[1★] David A. H. Buckley,[1] Darragh O'Donoghue,[1] Encarni Romero-Colmenero,[1] James O'Connor,[1] Piet Fourie,[1] Geoff Evans,[1] Craig Sass,[1] Lisa Crause,[1] Martin Still,[2,3] O. W. Butters,[4,5] A. J. Norton[4] and Koji Mukai[6,7]

[1]*South African Astronomical Observatory, PO Box 9, Observatory 7935, Cape Town, South Africa*
[2]*Mullard Space Science Laboratory, University College London, Holmbury St Mary, Dorking, Surrey RH5 6NT*
[3]*NASA Ames Research Center, Moffett Field, CA 94035, USA*
[4]*Department of Physics and Astronomy, The Open University, Walton Hall, Milton Keynes MK7 6AA*
[5]*Department of Physics and Astronomy, University of Leicester, Leicester LE1 7RH*
[6]*CRESST and X-ray Astrophysics Laboratory NASA/GSFC, Greenbelt, MD 20771, USA*
[7]*Department of Physics, University of Maryland, Baltimore county, 1000 Hilltop Circle, Baltimore, MD 21250, USA*

Accepted 2009 October 27. Received 2009 October 12; in original form 2009 July 7

ABSTRACT

We report optical spectroscopy and high-speed photometry and polarimetry of the *INTEGRAL* source IGRJ14536-5522 (=Swift J1453.4-5524). The photometry, polarimetry and spectroscopy are modulated on an orbital period of 3.1564(1) h. Orbital circularly polarized modulations are seen from ∼0 to ∼ −18 per cent, unambiguously identifying IGRJ14536-5522 as a polar. The negative circular polarization is seen over ∼95 per cent of the orbit, which is consistent (as viewed from the Earth) with a single-pole accretor. We estimate some of the system parameters by modelling the polarimetric observations.

Some of the high-speed photometric data show modulations that are consistent with quasi-periodic oscillations (QPOs) on the order of 5–6 min. Furthermore, for the first time, we detect the (5–6) min QPOs in the circular polarimetry. We discuss the possible origins of these QPOs. In addition, we note that the source undergoes frequent changes between different accretion states.

We also include details of HIgh-speed Photo-POlarimeter (HIPPO), a new high-speed photo-polarimeter, used for some of our observations. This instrument is capable of high-speed, multi-filtered, simultaneous all-Stokes observations. It is therefore ideal for investigating rapidly varying astronomical sources such as magnetic cataclysmic variables.

Key words: accretion, accretion discs – methods: analytical – techniques: polarimetric – binaries: close – novae, cataclysmic variables – X-rays: stars.

1 INTRODUCTION

The standard picture of a cataclysmic variable (CV) is a binary system consisting of a Roche lobe filling red dwarf (known as the secondary or the donor star) and an accreting white dwarf (the primary). CVs have orbital periods of typically a few hours, and mass transfer is caused by angular momentum loss [see e.g. Warner (1995) for a review of CVs]. Approximately 20 per cent of the known CVs are magnetic cataclysmic variables (mCVs), where the white dwarf has a strong magnetic field (see the catalogue of Ritter & Kolb 2003). These are further subdivided into two subtypes, namely intermediate polars (IPs) and polars, depending on the strength of the magnetic field of the white dwarf and the degree of synchronism between the white dwarf spin and the binary orbit [see the reviews given by Cropper (1990) and Patterson (1994)].

In polars, also known as AM Her systems, the white dwarf has a sufficiently strong magnetic field to lock the system into synchronous rotation and to completely prevent the formation of an accretion disc. Instead, the material from the secondary overflowing the Roche lobe initially falls towards the white dwarf following a ballistic trajectory until, at some distance from the white dwarf,

★E-mail: sbp@saao.ac.za

the magnetic pressure overwhelms the ram pressure of the ballistic stream, confining the flow until it eventually reaches the surface where it forms a hot shocked region.

It has long been known that CVs are a significant source of soft (<2 keV) and medium-energy (2–10 keV) X-rays (e.g. Patterson et al. 1984). Recent surveys with *INTEGRAL* show that CVs are also notable sources of hard (>20 keV) X-rays. A large fraction of these are made up of magnetic CVs and in particular IPs (see Barlow et al. 2006; Revnivtsev et al. 2008). Interestingly, out of the five asynchronous polars known, two are *INTEGRAL* sources.

IGRJ14536-5522 (=Swift J453.4-5524) was discovered as a hard X-ray source by *INTEGRAL* (Kuiper et al. 2006) and by *Swift*/Burst Alert Telescope (BAT) (Mukai et al. 2006a). A pointed *Swift*/XRT observation led to the identification with a *ROSAT* all-sky survey (RASS) source 1 RXS J145341.1-552146, and hence to its optical identification (Masetti et al. 2006). Revnivtsev et al. (2008) classify it as an IP.

Follow-up spectroscopy and photometry with Southern African Large Telescope (SALT) and with the South African Astronomical Observatory (SAAO) 1.9-m telescope showed that this object belongs to a rare subtype of magnetic CV: a hard X-ray bright polar or a soft IP (Mukai et al. 2006b). Further observations were clearly needed.

Here, we report on our optical photo-polarimetric and spectroscopic observations of IGRJ14536-5522. This paper is structured as follows. In Section 2, we describe the overall design of a new high-speed photo-polarimeter used for some of our observations. Section 3 gives an account of all our observations, followed by our analysis of the spectroscopic and photo-polarimetric observations in Sections 4 and 5, respectively. We finish with a discussion and summary in Section 6.

2 THE HIGH-SPEED PHOTO-POLARIMETER

SAAO's HIgh-speed Photo-POlarimeter (HIPPO) was designed and built in order to replace its highly successful but ageing single channel equivalent, namely the University of Cape Town (UCT) photo-polarimeter (Cropper 1985). Its purpose is to obtain simultaneous all-Stokes parameters, multi-filtered observations of unresolved astronomical sources. In addition, it is capable of high-speed photo-polarimetry in order to permit investigations of rapidly varying polarized astronomical sources. Of particular interest are mCVs. This is the first refereed publication of the instrument, and therefore we describe the overall instrument design, data acquisition and reduction here.

2.1 The optical design

Fig. 1 shows a schematic diagram of the optical layout of the polarimeter. Light from the telescope first encounters a field lens that produces a collimated beam. Within the collimated beam is placed a polarizing calibration filter wheel followed by superachromatic 1/4 and 1/2 waveplates. The polarizing calibration filter wheel consists of two linear polaroids, one circular polaroid (a linear followed by a 1/4 wave plastic retarder to produce a circularly polarized beam), a Lyot depolarizer and an open position. These filters are used for calibration and efficiency measurements of the instrument and/or the telescope. The 1/4 and 1/2 waveplates are also placed in the collimated beam in order to minimize any lateral modulation of the pupil image as the waveplates are rotated. A Thompson beamsplitter then produces the ordinary and extraordinary beams. All of the above polarizing optics are placed before any filters or apertures to avoid problems caused by metallic apertures or filters with residual stress birefringence.

Each beam has its own neutral density, colour filter and aperture wheels. The beams are focused at the aperture wheels by lenses at the top of each channel. Fabry lenses re-image the pupil on to two photo-multiplier tubes. There is also an eyepiece (used for initial alignment) and a dark slide on each channel.

The waveplates are contrarotated at 10 Hz and therefore modulate the ordinary and extraordinary beams. The modulation is sufficiently rapid that errors which arise as a result of variable atmospheric conditions or telescope guiding modulations are much reduced. In addition, modulations that occur as a result of wedge-shaped rotating elements, dirt on the rotating components or dichroism from refraction at the element surfaces appear mostly at harmonics that do not affect the measurement of polarization. The remaining sources of error are photon statistics, which

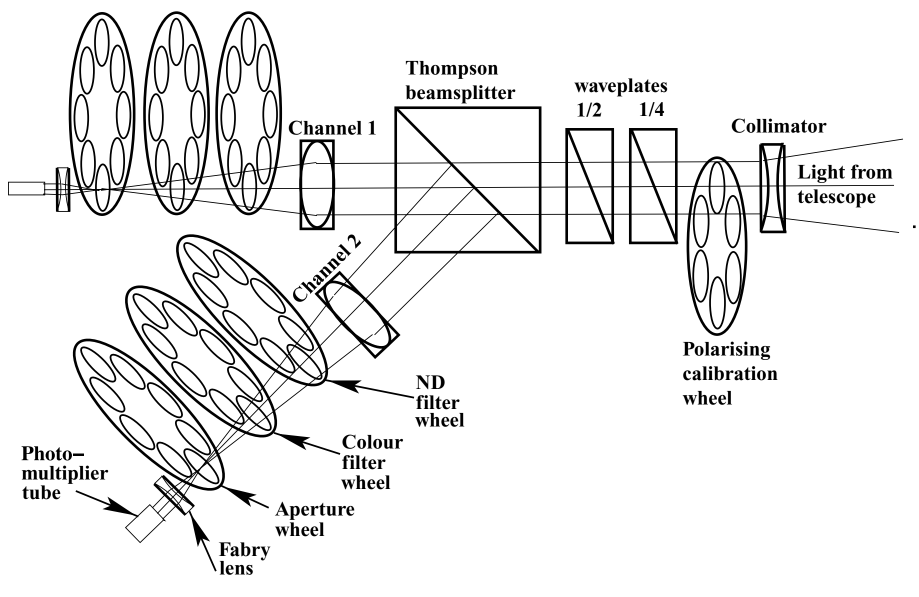

Figure 1. Optical layout of the polarimeter. Channel 1 is a copy of Channel 2.

can be minimized by collecting a larger number of photons, and instrument/telescope polarization, which can be measured by observing polarized and unpolarized standard stars in combination with the calibration filters. This recipe for measuring polarimetry is based on the work of Serkowski (1974). Measurements of all the Stokes parameters are made simultaneously from the modulated beams. As both beams are modulated, each provides an independent measurement of the polarization. Therefore, simultaneous two filter observations are possible. Linear- and circular-only modes are also possible by rotating only the 1/2 or 1/4 waveplates, respectively.

Serkowski (1974) provides the formalism for calculating the Stokes parameters from O and E beams that are modulated as a result of passing through two retarders in series. In our case, for constantly contrarotating 1/4 and 1/2 waveplates in series, the modulated intensities are given by

$$I'_{\mathrm{O}} = \frac{1}{2}\bigg(I + \frac{1}{2}Q[\cos 8\Psi_8 + \cos 4\Psi_4] + \frac{1}{2}U[\sin 8\Psi_8 - \sin 4\Psi_4] - V[\sin 6\Psi_6]\bigg)$$

$$I'_{\mathrm{E}} = \frac{1}{2}\bigg(I + \frac{1}{2}Q[-\cos 8\Psi_8 - \cos 4\Psi_4] + \frac{1}{2}U[-\sin 8\Psi_8 + \sin 4\Psi_4] + V[\sin 6\Psi_6]\bigg)$$

for the O and E beams, respectively. Where

$$\Psi_8 = 8\Psi - 4C^{(\frac{1}{2})} + 4C^{(\frac{1}{4})}$$

$$\Psi_6 = 6\Psi - 4C^{(\frac{1}{2})} + 2C^{(\frac{1}{4})}$$

$$\Psi_4 = 4\Psi - 4C^{(\frac{1}{2})}$$

and Ψ is the angle between the fast axis of the two waveplates and referenced to the 1/4 waveplate fast axis. $C^{(\frac{1}{2})}$ and $C^{(\frac{1}{4})}$ are the zero-point constant offsets for the 1/2 and 1/4 waveplates, respectively, and I, Q, U and V are the Stokes parameters. From these equations, one can see that the linear component of the polarization is modulated equally at the fourth and eighth harmonics of the rotation frequency. The circular component is modulated at the sixth harmonic. The linear polarization is measured by adding the amplitudes of the fourth and eighth harmonics and, similarly, by measuring the sixth harmonic for the circular polarization. A least-squares algorithm is used to obtain the amplitudes and phases of the harmonics. Correction factors are applied to each harmonic in order to compensate for the fact that the modulated signal is made up of a finite number of bins (100). Efficiency factors, to compensate for the slight wavelength dependence in retardance of the waveplates and instrumental polarization, are measured by observing polarized and unpolarized standard stars.

2.2 Data acquisition and reductions

The control and data acquisition software is written in C and is hosted by an industrial PC. The photometer counts (X2), minute and second time pulses and 1/2+1/4 waveplate pulses are handled by real time C code in order to ensure correct and absolute timely recording of the data. The real time code is driven by a 1 ms time interval interrupt driven by a 1 kHz signal from the time service provided by the Observatory. At every interrupt, the status of the waveplate pulses, time pulses and the photometer buffers is recorded. These data are then sent to the user C code, where on-the-fly data reductions are performed. The 1 ms data stream is also saved to disc for later off-line data reduction. With a data rate of 1 kHz, the 10 Hz rotating waveplates are sampled 100 times per revolution. Therefore, every 0.1 s a polarization measurement is made. Off-line data reductions permit binning of the data to any integer multiple of 0.1 s.

3 OBSERVATIONS

Table 1 shows a log of all the observations of IGRJ14536-5522.

3.1 Optical spectroscopy

Spectroscopic observations of IGRJ14536-5522 were made during 2007 July on the 1.9-m telescope located on the Sutherland site of the SAAO, using the Cassegrain spectrograph with the SITe1 CCD (1752 × 266 × 15 μm pixels). The higher resolution grating was chosen in order to cover the Hβ, He II and Hγ emission lines. The lower resolution grating was chosen in order to cover a broader optical wavelength range. Flat-field spectra were obtained at the beginning and/or end of each night and wavelength calibration was provided by observing a CuAr lamp approximately every 20–25 min. Spectrophotometric flux standards were also observed, allowing flux calibration. Data reductions made use of the standard tools available through IRAF.

SALT RSS spectra were obtained when the system was in a lower state between 2006 May 14 and June 9. These observations were presented in Mukai et al. (2006a) and have been listed here for completeness and for comparison.

3.2 Optical polarimetry

IGRJ14536-5522 was observed polarimetrically on the SAAO 1.9-m telescope during the commissioning week of the HIPPO in 2008 February and March and then later in 2008 April. The HIPPO was operated in its simultaneous linear and circular polarimetry and photometry mode (all-Stokes). White light observations (3500–9000 Å) were defined by the response of the two RCA31034A GaAs photomultiplier tubes, whilst for others a broad blue band (3500–5500 Å) BG39 filter, a broad red band (5700–9000 Å) OG570 filter or *B,V,R,I* filters were used.

Several polarized (HD 80558, HD 111579, HD 111613, HD 147084, HD 126593, HD 147084, HD 160529, HD 298383, HD 110984) and non-polarized (HD 90156, HD 100623) standard stars (Hsu & Breger 1982; Bastien et al. 1988) were observed in order to calculate the position angle offsets, instrumental polarization and efficiency factors. Background sky polarization measurements were also taken at frequent intervals during the observations. Data reduction then proceeded as outlined in the previous sections.

3.3 Optical photometry

IGRJ14536-5522 was observed photometrically with the UCTCCD in 2006 as part of the polarimetric observations in 2008 and with SALTICAM in 2008. The observations are not absolutely photometrically calibrated.

4 SPECTROSCOPIC ANALYSIS

4.1 The mean spectrum

Fig. 2 shows the average of the spectra taken when the system was in a higher state (upper spectrum) and when it was observed to be in a lower state two weeks later during 2007 July (lower spectrum).

Table 1. Table of observations. Cass Spect is the Cassegrain spectrograph, 1.9 m, and HIPPO are the 1.9-m telescope and the HIgh-speed Photo-POlarimeter, respectively, of the SAAO. OG570 and BG390 are broad-band red and blue filters, respectively. SALTICAM is the CCD camera of the Southern African Large Telescope. UCTCCD is the University of Cape Town CCD camera. RSS is the Robert Stobie Spectrograph. Observed bright and faint states are indicated by [h] and [l] in the last column. [M] denotes observations originally published in Mukai et al. (2006a).

Date	Telescope	Instrument	Spectral range/ filter	Resolution (Å)	No. of spectra	Integration times (s)	Data set length (orbits)
2006 Sept 14/15	1.9 m	UCT CCD	Clear	-	-	60	~0.85[hM]
2006 Sept 15/16	1.9 m	UCT CCD	Clear	-	-	60	~0.37[hM]
2006 Sept 17/18	1.9 m	UCT CCD	Clear	-	-	60	~0.72[hM]
2006 Sept 18/19	1.9 m	UCT CCD	Clear	-	-	60	~0.82[hM]
2006 May/Jun 14-9	SALT	RSS	5930–7212 Å	1	31	600	~0.9[lM]
2007 Jul 6/7	1.9 m	Cass Spect	4000–5000 Å	1	42	600	~2.1[h]
2007 Jul 8/9	1.9 m	Cass Spect	4000–5000 Å	1	42	600	~2.1[h]
2007 Jul 9/10	1.9 m	Cass Spect	4000–5000 Å	1	39	600	~2.0[h]
2007 Jul 10/11	1.9 m	Cass Spect	3750–7800 Å	4	42	500	~2.0[h]
2007 Jul 25/26	1.9 m	Cass Spect	4000–8000 Å	4	9	1200	~1.0[l]
2008 Feb 27/28	1.9 m	HIPPO	Unfiltered	-	-	1ms,0.1	~1.2[h]
2008 Feb 28/29	1.9 m	HIPPO	OG570, BG39	-	-	1ms,0.1	~1.2[h]
2008 Feb 29/1	SALT	SALTICAM	Clear	-	-	0.1	~0.35[h]
2008 Mar 1/2	SALT	SALTICAM	Clear	-	-	0.1	~0.15[h]
2008P Mar 1/2	1.9 m	HIPPO	*B,I*	-	-	1ms	~1.2[h]
2008 Mar 2/3	SALT	SALTICAM	Clear	-	-	0.1	~0.17[h]
2008 Mar 2/3	1.9 m	HIPPO	*B,R*	-	-	1ms	~1.2[h]
2008 Apr 3/4	1.9 m	HIPPO	*B,I*	-	-	1ms, 0.1s	~1.2[h]
2008 Apr 5/6	1.9 m	HIPPO	*B,V,R,I*	-	-	1ms, 0.1s	~1.5[h]
2008 Apr 7/8	1.9 m	HIPPO	Clear, *B,I*	-	-	1ms, 0.1s	~1.2[h]
2008 May 7/8	SALT	SALTICAM	*U*	-	-	0.1	~0.13[h]
2008 May 7/8	SALT	SALTICAM	*B*	-	-	0.1	~0.26[h]
2008 May 9/10	SALT	SALTICAM	*V*	-	-	0.1	~0.23[h]
2008 May 13/14	SALT	SALTICAM	*R*	-	-	0.1	~0.3[h]
2008 May 17/18	SALT	SALTICAM	*B*	-	-	0.1	~0.26[h]
2008 May 18/19	SALT	SALTICAM	*V*	-	-	0.1	~0.1[h]

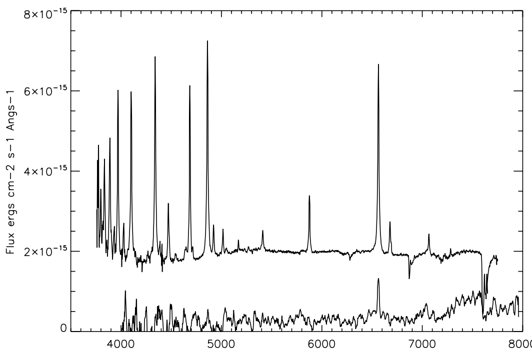

Figure 2. Average of the low-resolution spectra. Upper and lower average spectra are made from the observations taken on 2007 July 10/11 (during a higher state) and 25/26 (during a lower state), respectively. The lower state data have been magnified by 10.

These observations were made with the SAAO 1.9-m telescope. The higher state spectrum is very typical for a polar (see e.g. QS Tel: Rosen et al. 1996, HU Aqr: Schwope, Mantel & Horne 1997), i.e. it exhibits Balmer emission lines (Hα–H11) as well as neutral helium (He I $\lambda\lambda$ 4026, 4387, 4471, 4713, 4922, 5016, 5048, 5876, 6678, 7065 Å), ionized helium (He II $\lambda\lambda$ 4542, 4686, 5411), Ca II (3933 Å), blended C III, O II, N III (4640 Å) and Fe I (5172 Å). The phase-resolved low-resolution spectra clearly display bright and faint phases (not shown).

4.2 A spectroscopic ephemeris for the secondary

We measured the radial velocity of the Hα emission line in our 2007 July observations using a single-Gaussian convolution method. These results were then combined with the same measurements made by Mukai et al. (2006a) of their 2006 June observations. A χ^2 minimization technique was then used in order to search for any periods. A period of 3.1564(1) h was detected which is consistent with that found by Mukai et al. (2006a) and recognized as the orbital period. The period error arises as a result of not being able to distinguish between aliases.

Fig. 3 shows the Hα radial velocity curve folded on the 3.1564 h period with arbitrary phasing. We measure a gamma velocity of $-7.3(1)$ km s^{-1} and a semi-amplitude of 144.9(2) km s^{-1}. The numbers in brackets are the 1σ standard deviations of a sine fit to the radial velocities. The higher and lower state data are distinguished by the crosses and diamonds, respectively. Note that the higher state data appear to have a generally higher velocity than the lower state data. We attribute this to different emission regions contributing to the line emission when in different states: the irradiated face of the secondary star dominates the emission-line profile during lower states, but the emission lines become multi-component during higher states (see e.g. UW Pic: Romero-Colmenero et al. 2003). Hence, the multi-component nature of the emission lines has probably biased our gamma velocity measurement due to asymmetric line profiles.

In order to derive a zero-point for the ephemeris we analysed our higher resolution spectroscopic data. Fig. 4 shows these data, taken

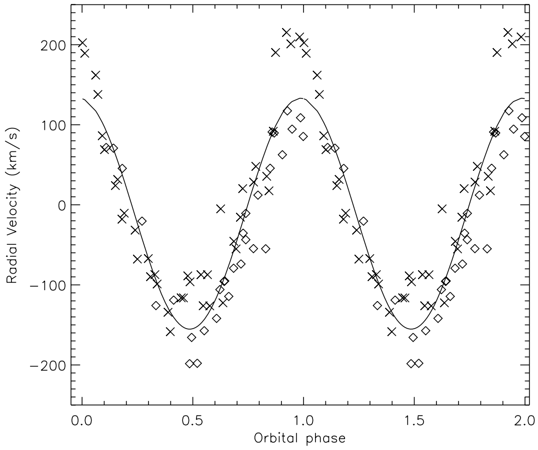

Figure 3. The Hα radial velocity curve of IGRJ14536-5522 folded on the 3.1564 h period with arbitrary phasing. Crosses and diamonds are the higher state 2007 and the lower state 2006 observations, respectively.

in 2007 July, phased and folded on the above-detected period and centred on the He II 4686 Å line. These observations show the multi-component nature more clearly (described in more detail below). In particular, a bright narrow component can be seen (indicated by the dashed curve), which is commonly associated with the irradiated face of the secondary star. We fitted multi(three)-Gaussian profiles to the trailed spectra and calculated the radial velocities of the three visible components as a function of phase. A best sinusoidal fit to the narrow component was used in order to derive the time of blue–red crossing and hence the time of inferior conjunction of the secondary star. Accordingly, this in turn is used to give the epoch to our ephemeris:

$$T(\mathrm{HJD}) = 245\,4290.147\,23(8) + 0.131\,517(4)E.$$

The number enclosed in brackets (on the epoch) is the formal 1σ error measurement. However, we note that the true superior conjunction of the secondary may be offset by a value that is larger than the quoted error if the irradiated face of the secondary is not symmetric about the line of centres of the two stars.

We measure a gamma velocity and semi-amplitude of $-26.0(3)$ and $80.8(4)$ km s^{-1}, respectively, for the narrow component. The numbers in brackets are the 1σ standard deviations of a sine fit to the radial velocities. Henceforth, all our observations are phased on the above ephemeris.

4.3 The trailed spectra and Doppler tomograms

Fig. 4 shows our He II trailed spectra, the corresponding Doppler tomogram (Marsh & Horne 1988) and the reconstructed trailed spectra of IGRJ14536-5522. The spectra were phase-folded on the ephemeris derived above, continuum subtracted, and then the Doppler tomography code of Spruit (1998) was used.

We have also calculated Hβ and Hγ Doppler tomograms (not shown). These were found to be very similar to the He II Doppler tomogram, but the trailed spectra do not show the narrower components as clearly. Therefore, we present only the He II observations and the corresponding interpretation.

The He II trailed spectra clearly display the multiple components that have been seen to some extent in other polars (e.g. Schwope et al. 1995; Rosen et al. 1996). From Fig. 4, a narrow component (indicated by the dashed curve) is visible throughout the whole orbit and is generally recognized as emission from the irradiated face of the secondary star. The fact that it is visible throughout the whole orbit suggests a relatively low inclination, although the radial velocity amplitudes are consistent with more moderate inclinations (see e.g. V834 Cen: Potter et al. 2004).

There is possibly a second narrow component that is most visible where it crosses and merges (indicated by diagonal lines) with the narrow component from the secondary at phases ∼0.25 and ∼0.75. There also appears to be a broad but fainter underlining component that reaches maximum blueshift velocities of ~ -1000 km s^{-1} at phase ∼0.5, and it remains discernible with maximum redshift just before phase ∼1.0. This fits the general picture of emission from a ballistic accretion stream which then accelerates and becomes magnetically channelled before reaching the surface of the white dwarf (producing the broad component).

The He II Doppler tomogram in Fig. 4 shows the typical features of a moderately inclined polar. In particular, emission is seen at the expected location of the irradiated face of the secondary, approximately centred on x-velocity ∼0 km s^{-1} and y-velocity ∼100 km s^{-1}. The x-velocity appears to be slightly negative offset from 0. This can be explained as being due to the leading edge of the secondary being more illuminated by the hot accretion region on the surface of the white dwarf, which also leads in orbital phase (e.g. V834 Cen: Potter et al. 2004), although we cannot rule out that it may also be as a result of inaccuracies in the determination of the gamma velocity and/or the phasing of inferior conjunction on the secondary. The tomogram also shows emission at the expected location of the ballistic accretion stream, seen to start at roughly the location of the secondary and curving away towards more negative x- and y-velocities. There is also a very faint underlying component seen protruding from zero velocities to low negative velocities.

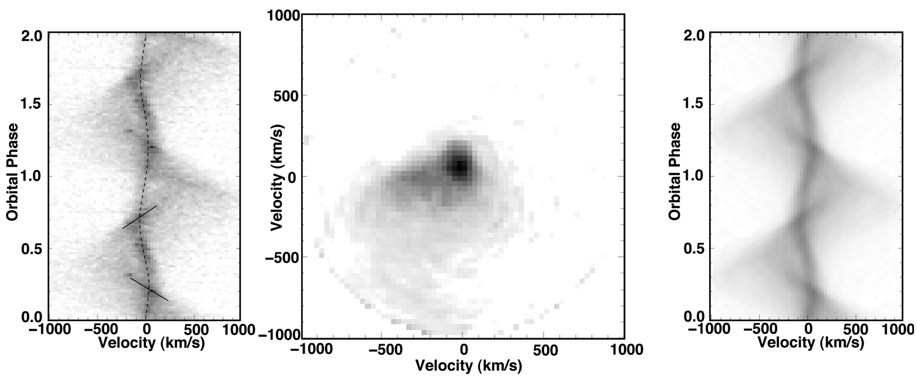

Figure 4. From left to right: He II trailed spectra phase-folded on the derived ephemeris, the resulting Doppler tomogram and the reconstructed trailed spectra.

This has also been seen in other polars (e.g. Hu Aqr: Schwope et al. 1997) and is generally explained as emission from accreting material where it starts to be threaded by the magnetic field of the white dwarf.

5 PHOTO-POLARIMETRIC ANALYSIS

5.1 The photometry

The left-hand plots of Fig. 5 show the photometric observations of IGRJ14536-5522 taken on 2008 April 5 (top four plots) and April 7 (last plot), phased on the spectroscopic ephemeris derived in Section 4.2. The April 5 observations were obtained by interleaving 60-s integrations between the *B* and *V* filters and the *R* and *I* filters on Channels 1 and 2 of the polarimeter, respectively. They are, therefore, effectively simultaneous. Conditions were photometric during these observations. The source was in a higher state.

5.1.1 The orbital modulation and the dip

As can be seen from Fig. 5, the orbital modulation is single-humped, which can be attributed to the beaming of cyclotron emission from a single accretion spot on the surface of the white dwarf. The orbital intensity minimum occurs when the emission region is most face-on. The single-humped morphology also implies a moderate inclination for the system (see e.g. Ferrario & Wickramasinghe 1990; Potter, Hakala & Cropper 1998).

The orbital intensity minimum is cut into by a narrow dip at approximately phase ∼0.97. This dip is also seen in the polarimetry light curves (Fig. 5, right-hand side). Considering the accuracy of the phasing of the spectroscopic ephemeris (Section 4.2), the narrow dip could be due to an eclipse of the white dwarf by the secondary star. However, this scenario is not consistent with the results of our spectroscopic analysis and polarimetric modelling (Sections 4.3 and 5.2, respectively), which favour moderate inclinations. Therefore, it is more likely that the dip arises as a result of absorption by material in the accretion stream and/or the accretion column directly above the emission region when we see it most face-on (see e.g. Bridge et al. 2002).

5.1.2 The photometric QPOs and flickering

A close inspection of the photometry in Fig. 5 reveals short-period modulations throughout the orbit that are mostly consistent with being due to noise or flickering. However, detailed Fourier analysis of all of our photometry reveals that some of our data sets show significant singularly persistent peaks that are consistent with quasi-periodic oscillations (QPOs).

An example data set is shown in the left-hand (a) plot of Fig. 6 from 2008 February 28. We analysed the data set by first splitting it into ∼40 min sections with an overlap of 85 per cent. Next, each section of data was normalized to a best-fitting second-order polynomial before being subjected to the Fourier analysis. The results are shown as a trailed amplitude spectrum in the left-hand (b) plot of Fig. 6. In this grey-scale plot, the darker areas correspond

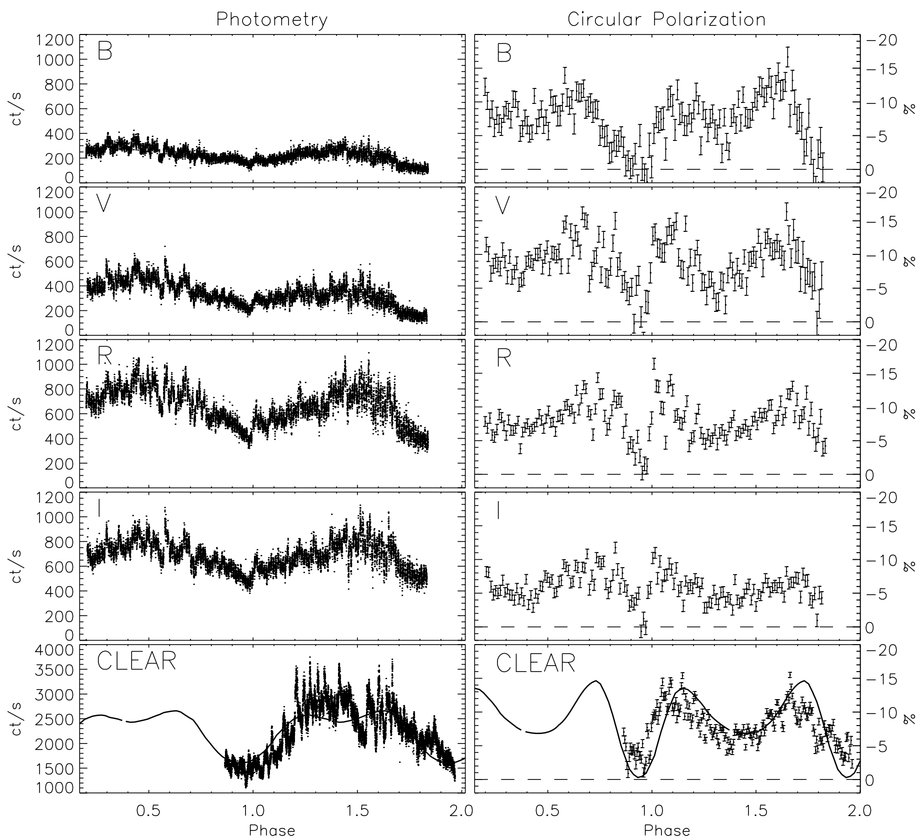

Figure 5. The photometric and polarimetric data phased on the spectroscopic ephemeris derived in Section 4.2. The upper four plots are simultaneous *B, V, R* and *I* filtered observations of 2008 April 5 whilst the bottom plots were made with the clear filter on 2008 April 7. Solid curves represent the model fit (see Section 5.2).

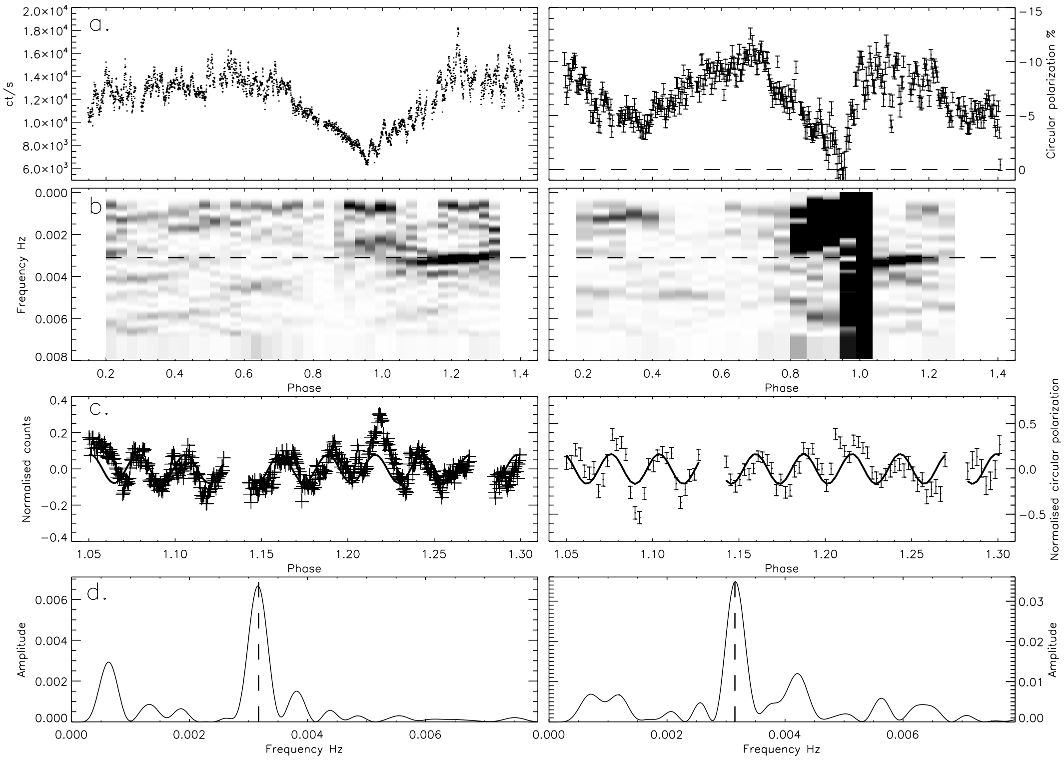

Figure 6. Left-hand plots (a–d): the photometry, the corresponding trailed amplitude spectra, the normalized photometry for the phase range 1.0–1.3 and its corresponding amplitude spectra, respectively. The solid curve is the least-squares fit using the frequency derived from the trailed spectra (dashed line). Right plots: as in the left plots but for the circular polarization. Data set from 2008 February 28.

to larger amplitudes. Between Phases 0.2 and 1.0, the amplitude spectra do not show any significant peaks, which indicates that the variations are mostly flickering or noise. However, there is a significant dominating signal centred on 0.0032(1) Hz (5.2 min, indicated by the dashed line) between phases 1.0 and 1.3. This is clear evidence of a QPO. The 2008 April 7 data set also shows clear evidence of a QPO [Fig. 7, left (a+b) plots] at a similar period [0.0028(1) Hz, ∼5.9(3) min] centred on the same phase range (∼1.2) as well as a lower harmonic [0.00136(15) Hz], both indicated with dashed lines.

In the left-hand (c) plot of Fig. 6, we show the normalized photometry during the phase range that is dominated by the QPO. Overplotted are the least-squares fit of the QPO frequencies. As one can see, the February 28 photometric QPO is very well described by the single dominant frequency as found in the trailed amplitude spectra. The 2008 April 7 photometric QPO [Fig. 7, left-hand (c) plot] shows a more variable amplitude compared to the February 28 QPO. This then explains why the trailed amplitude spectra show two frequencies for the QPO, one being the harmonic of the other. The left-hand (d) plots of Figs 6 and 7 show the corresponding amplitude spectra for the QPO-dominated phase range. The QPOs are discussed further in Section 6.2.

5.2 The polarimetry

The right-hand plots of Fig. 5 show the polarimetric (circular) observations of IGRJ14536-5522 taken on 2008 April 5 (top four plots) and April 7 (bottom plot), phased on the spectroscopic ephemeris derived in Section 4.2. These were generated from the same data set as the photometry presented in the left-hand plots. We were unable to detect any linear polarization.

The circular polarization curve is double-humped and negative throughout the orbit, which is consistent with emission from a single accretion region in a moderately inclined system. The polarization reaches maximum negative values of ∼15 per cent, with the peaks of the humps occurring at orbital phases ∼0.1 and ∼0.7. There is also a narrow dip at phase ∼0.97, where the polarization reaches a minimum of zero. This is coincident with the narrow dip seen in the photometry, thus supporting the hypothesis that the emission being absorbed is cyclotron radiation from the accretion region (Section 5.1.1). The phasing of the dip implies that the location of the accretion region must be close to the line of centres of the two stars. In addition, there is a broad minimum centred on the narrow dip, which is typically caused by the beaming of the cyclotron radiation at those phases where the line of sight most closely approaches the axis of the column (Barret & Chanmugam 1984; Wickramasinghe & Meggitt 1985).

5.2.1 *The system geometry*

We investigated the system geometry further by modelling the photo-polarimetry. We constructed a single-arc model assuming accretion along dipole field lines as in Potter et al. (1997). A magnetic field of 20 MG was assumed and the cyclotron flux was calculated using the stratified accretion shock grids of Potter et al. (2002). We considered only the clear filter data because there does not appear to be any obvious wavelength dependence in the multi-filtered observations. Consequently, different values for the magnetic field strength and different shock models cannot be investigated. However, the results of this model are largely independent of our choice of the magnetic field strength.

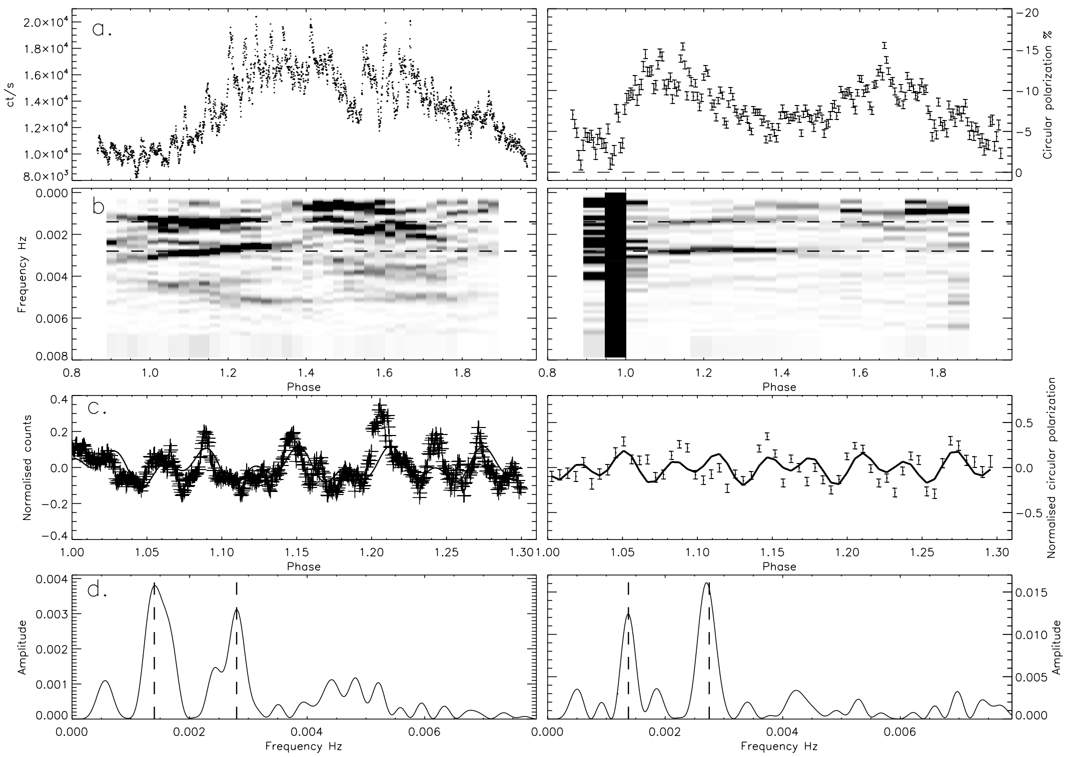

Figure 7. As in Fig 6 for the 2008 April 7 data set.

The values for the parameters describing the inclination, dipole offset angle and location, shape and size of the accretion region were explored by comparing each resulting light curve to the data. The most successful set of parameters integrated the emission from an arc-shaped region extending from 170° to 230° in magnetic longitude and 10° from the magnetic pole with a system inclination of 50°. The magnetic dipole was offset by an angle of 10° from the white dwarf spin axis. A constant unpolarized background of 1000 ct s^{-1} was assumed.

We found that the model gave poor reproductions of the data for inclinations outside a range of 45°−55°, when either the extent in phase or the double-humped morphology of the circular polarization was poorly reproduced. The solid curves in the lower two plots of Fig. 5 show the results of the best model parameters overplotted on the observations. The model has the accretion region most face-on at phase ∼0.95 and least face-on at phase ∼0.45.

5.2.2 *The polarized QPOs and flickering*

We analysed our circular polarimetric data in the same manner as that of the photometry. The data and results for the 2008 February 28 are shown in the right-hand plots of Fig. 6. As can be seen from the right-hand (b) plot, the trailed amplitude spectra are consistent with mostly noise and/or flickering between phases 0.2 and 1.0. However a QPO centred on 0.0031(1) Hz [5.4(3) min] is clearly evident between phases 1.05 and 1.2. The QPO period is consistent within the errors to that of the photometric QPO.

The right-hand plots of Fig. 7 show the Fourier analysis of the circular polarimetric data taken on 2008 April 7. Once again, the trailed amplitude spectra display the same characteristics as the photometry, i.e. a dominant frequency is seen to be centred on 0.0028(1) Hz [5.9(3) min] and a lower harmonic at 0.0015(1) Hz (both indicated by dashed lines) during the phase range 1.0–1.3.

In the right-hand (c) plots of Figs 6 and 7, we show the normalized circular polarimetry during the phase range that is dominated by the QPOs. Overplotted are the least-squares fit of the QPO frequencies. As one can see, the circularly polarized QPOs share the same characteristics as the photometric QPOs, namely the February 28 circularly polarized QPO is very well described by the single dominant frequency found in the trailed amplitude spectra. Furthermore, the 2008 April 7 circularly polarized QPO shows a more variable amplitude compared to the February 28 QPO, thus requiring a harmonic frequency to better characterize the data. The QPOs are discussed further in Section 6.2.

6 DISCUSSION AND SUMMARY

6.1 Object classification and system geometry

Our optical spectroscopy and high-speed photo-polarimetry of the *INTEGRAL* source IGRJ14536-5522 (=Swift J453.4-5524) unambiguously confirm its identification as a polar. Negative circular polarization is seen over all of the orbit, which is consistent with a single-pole accretor at a moderate inclination. We estimate some of the system parameters by modelling the polarimetric observations. The most successful model integrated the emission from an arc-shaped region extending from 170° to 230° in magnetic longitude and 10° from the magnetic pole. The system inclination was found to be in the range of 45°–55° with a magnetic dipole offset angle of 10°.

6.2 The QPOs and flickering

Our high-speed photo-polarimetry shows flickering on minute timescales. Furthermore, for the first time, we detect QPOs in the photometry and circular polarimetry.

Photometric variations on the time-scales of minutes are a common feature of many polars, from X-rays to infrared (e.g. Szkody & Margon 1980; Watson, King & Williams 1987), and have been characterized as flickering, fluctuations, QPOs or erratic QPOs according to different authors. In general (although not always strictly true), QPOs describe variations that show some coherence over a period of time. They mainly cluster in time-scales in the range of a few seconds (1–5) or minutes (4–10). The (1–5 s) QPOs are of low amplitude and have been observed in the optical in only a few polars (e.g. V834 Cen, AN Uma and VV Pup). The larger amplitude (4–10 min) QPOs seem to be a general feature of most polars. By eye, they can appear to show some sort of coherence, but fail to show any significant singularly persistent peaks under Fourier analysis. Instead, groupings of periods are seen and are often referred to as QPO-like. Flickering and fluctuations best describe variations that do not show any periodic behaviour.

There is evidence that the 4–10 min QPOs may consist of the superposition of regular periodic oscillations: Bonnet-Bidaud, Somova & Somov (1991) report on observations of AM Her during an intermediate brightness state where they find fluctuations to be nearly periodic, with a period increasing from 250 to 280 s. They reason that they observed AM Her in a transition from bright to faint state where a given accretion rate is able to excite stable oscillations. Alternatively, during the higher state, many oscillations may be present but masked by the superposition of different modes corresponding to different accretion tubes. Therefore, during the transition, the accretion rate decreases, reducing the number of accretion tubes until finally only one unique tube contributes to the emission.

Ultimately, the photometric oscillations are caused by variations in the accretion flow. There are several theories/models that attempt to explain the variations. King (1989) remarks that the (4–10 min) periods are characteristic of a dynamical time at the photosphere of the companion. Irradiation of the region near the L_1 point will result in the formation of an ionization front, which will tend to oscillate and therefore modulate the accretion. Other models involve the capture of inhomogeneities of the accretion flow at the capture radius (Kuijpers & Pringle 1982) and accretion gate mechanisms (Patterson, Williams & Hiltner 1981).

The short-period QPOs (1–5 s) have been observed in nearly six systems (e.g. V834 Cen, AN Uma and VV Pup). Langer, Chanmugam & Shaviv (1982) realized that the 1–5 s oscillations were consistent with the cooling time-scales for white dwarf radiated shock waves and thus QPOs are potentially powerful probes of the radiative shocks. Observations of VV Pup (Larson 1989) conclusively demonstrated that the QPOs arose in a region near the shock emission region on the white dwarf.

From our results presented in Figs 6 and 7, it is clear that IGRJ14536-5522 exhibited photometric and polarized QPOs (5–6 min) on two separate occasions. Additionally, the fact that we observe the QPOs oscillations in the polarimetry, unequivocally places the emission site at the cyclotron emitting shock region. Furthermore, the QPOs were seen during phases 1.0–1.3 only. We propose that the superposition of the oscillations arising from numerous accretion tubes (similar to the mechanism of Bonnet-Bidaud et al. 1991) applies to IGRJ14536-5522. However, instead of a reduced accretion state leading to a reduced number of accretion tubes, we suggest that for most of the orbit the superposition of emission from many accretion tubes leads to the observed flickering. However, during the phase interval 1.0–1.3 we preferentially see the trailing edge of the accretion region as the white dwarf rotates. The leading part of the accretion region is effectively shielded from our view by its trailing edge for this phase interval. Consequently, we observe a singular QPO corresponding to a singular accretion tube.

Our observations of IGRJ14536-5522 indicate that it undergoes relatively frequent changes in accretion state, making it a good candidate for capturing it in transition and testing this scenario further. If QPOs are also present in the X-rays, then IGRJ14536-5522 is an ideal source for investigating the two dominating shock cooling mechanisms, i.e. bremsstrahlung and cyclotron cooling.

Finally, we would like to note the importance of optical follow-up observations of candidate CV *INTEGRAL* sources, in particular with photometry and/or polarimetry. It has been noted that many CVs detected by *INTEGRAL* are IPs, both new and re-discoveries (see e.g. Barlow et al. 2006; Revnivtsev et al. 2008). However, as Pretorius (2009) points out, it is only through follow-up observations that unequivocal identifications can be made. A case in point is IGRJ14536-5522, which had been assumed to be an IP (see e.g. Revnivtsev et al. 2008) even though a spin period had not been detected.

ACKNOWLEDGMENTS

We thank the anonymous referee for comments and suggestions that have significantly improved the paper.

This material is based upon work supported financially by the National Research Foundation. Any opinions, findings and conclusions or recommendations expressed in this material are those of the author(s) and therefore the NRF does not accept any liability in regard to thereto.

Some of the observations reported in this paper were obtained with the SALT, a consortium consisting of the National Research Foundation of South Africa, Nicholas Copernicus Astronomical Center of the Polish Academy of Sciences, Hobby Eberly Telescope Founding Institutions, Rutgers University, Georg-August-Universitt Göttingen, University of Wisconsin – Madison, Carnegie Mellon University, University of Canterbury, United Kingdom SALT Consortium, University of North Carolina – Chapel Hill, Dartmouth College, American Museum of Natural History and the Inter-University Centre for Astronomy and Astrophysics, India.

REFERENCES

Barlow E. J., Knigge C., Bird A. J., Dean A. J., Clark D. J., Hill A. B., Molina M., Sguera V., 2006, MNRAS, 372, 224
Barret P. E., Chanmugam G., 1984, ApJ, 278, 298
Bastien P., Drissen L., Menard F., Moffat A. F. J., Robert C., St-Louis N., 1988, AJ, 95–900
Bonnet-Bidaud J. M., Somova T. A., Somov N. N., 1991, A&A, 251, L27
Bridge C. M. et al., 2002, MNRAS, 336, 1129
Cropper M. S., 1985, MNRAS, 212, 709
Cropper M. S., 1990, Space Sci. Rev., 54, 195
Ferrario L., Wickramasinghe D. T., 1990, ApJ, 357, 582
Hsu J. C., Breger M., 1982, ApJ, 262, 732
King A. R., 1989, MNRAS, 241, 365
Kuijpers J., Pringle J. E., 1982, A&A, 114, L4
Kuiper L., Keek S., Hermsen W., Jonker P. G., Steeghs D., 2006, Astron. Telegram 684
Langer S. H., Chanmugam C., Shaviv G., 1982, ApJ, 258, 289
Larson S., 1989, A&A, 217, 146
Marsh T. R., Horne K., 1988, MNRAS, 235, 269
Masetti N. et al., 2006, A&A, 459, 21
Mukai K. et al., 2006a, Astron. Telegram 686
Mukai K., Markwardt C., Tueller J., Buckley D., Potter S., Still M., Swift/BAT Team, 2006b, A&AS, 209, 0912
Patterson J., 1994, PASP, 106, 209

Patterson P., Williams G., Hiltner W. A., 1981, ApJ, 245, 618
Patterson J., Lamb D. Q., Fabbiano G., Raymond J. C., Beuermann K.Swank J., White N. E., 1984, ApJ, 279, 785
Potter S. B., Cropper M. S., Mason K. O., Hough J. H., Bailey J. A., 1997, MNRAS, 285, 82
Potter S. B., Hakala P. J., Cropper M., 1998, MNRAS, 297, 1261
Potter S. B., Ramsay G., Wu K., Cropper M., 2002, in Gänsicke B. T., Beuermann K., Reinsch K., eds, ASP Conf. Ser. Vol. 262, The Physics of Cataclysmic Variables and Related Objects. Astron. Soc. Pac., San Francisco, p. 165
Potter S. B., Romero-Colmenero E., Watson C. A., Buckley D. A. H., Phillips A., 2004, MNRAS, 348, 316
Pretorius M. L., 2009, MNRAS, 395, 386
Revnivtsev M., Sazonov S., Krivonos R., Ritter H., Sunyaev R., 2008, A&A, 489, 1121
Romero-Colmenero E., Potter Stephen B., Buckley D. A. H., Barrett P. E., Vrielmann S., 2003, MNRAS, 339, 685
Rosen S. R. et al., 1996, MNRAS, 280, 1121
Ritter H., Kolb U., 2003, A&A, 404, 301
Schwope A. D., Thomas H.-C., Beuermann K., Burwitz V., Jordan S., Haefner R., 1995, A&A, 293, 764
Schwope A. D., Mantel K.-H., Horne K., 1997, A&A, 319, 894
Serkowski K., 1974, in Gehrels T., ed., Planets, Stars and Nebulae Studied with Photopolarimetry. University of Arizona, Tucson, p. 135
Spruit H. C., 1998, preprint (astro-ph/9806141)
Szkody P., Margon B., 1980, ApJ, 236, 862
Warner B., 1995, Cataclysmic Variable Stars, Cambridge Astrophysics Series 28. Cambridge Univ. Press, Cambridge
Watson M. G., King A. R., Williams G. A., 1987, MNRAS, 226, 867
Wickramasinghe D. T., Meggitt S. M. A., 1985, MNRAS, 214, 605

This paper has been typeset from a TEX/LATEX file prepared by the author.